Resonance enhanced multiphoton ionization probing of H atoms and CH₃ radicals in a hot filament chemical vapour deposition reactor

James A. Smith, Moray A. Cook, Stephen R. Langford, Stephen A. Redman, Michael N.R. Ashfold*

School of Chemistry, University of Bristol, Bristol BS8 1TS, UK

Abstract

Resonance enhanced multiphoton ionization spectroscopy has been used to provide spatially resolved in situ measurements of H atom and CH₃ radical relative number densities and the local gas temperature in a hot filament reactor used for diamond chemical vapour deposition (CVD). Parameters varied include the hydrocarbon (CH_4 and C_2H_2), the hydrocarbon/H_2 process gas mixing ratio, the total pressure and flow rate, and the temperatures of both the filament and substrate. H atom number densities are observed to be a maximum at the hot filament surface, to be independent of the H_2 pressure, $p(H_2)$, in the range 5–55 Torr, and to drop monotonically with increasing radial distance from the filament, d. In contrast, the CH₃ radical number density arising both in dilute CH_4/H_2 and C_2H_2/H_2 gas mixtures is found to scale with the hydrocarbon input gas pressure, and to be rather constant for $d < 4$ mm and to decline thereafter. These direct measurements serve to reinforce the consensus view that H atom production during diamond CVD in a hot filament reactor arises as a result of dissociative adsorption on the hot filament surface, whereas CH₃ radical formation is dominated by gas phase reactions both when using CH_4 and C_2H_2 as the carbon source gas. The formation mechanism of CH₃ radicals in a hot filament reactor operating with C_2H_2/H_2 gas mixtures is considered further. © 2000 Elsevier Science S.A. All rights reserved.

Keywords: Diamond chemical vapour deposition; Laser probing; H atoms; CH₃ radicals

1. Introduction

Chemical vapour deposition (CVD) is now a well established route for forming polycrystalline diamond films, which are finding ever increasing roles, for example, as hard wear resistant coatings, as a window material with unprecedented infrared transmission, in thermal management, and in an expanding range of electronic and electrochemical applications [1,2]. Most diamond CVD involves activation of a dilute hydrocarbon/H_2 mixture (e.g. 1% CH_4 in H_2) at a pressure of a few tens of Torr, and subsequent growth on the chosen substrate material maintained at the necessary elevated process temperature (typically ~800°C) [3]. Activation may be thermal, as in the simple hot filament (HF) reactor, or plasma (e.g. microwave) enhanced. The formation of H atoms in such environments is vital to successful diamond growth. These H atoms are credited with several crucial roles. For example, they initiate gas phase reactions necessary for creating the reactive carbon containing species (e.g. CH₃ radicals), which adsorb onto,

and react with, the surface, thereby extending the growing diamond lattice. This addition reaction requires the incident CH₃ species to find a vacant surface site. Since the growing surface is continually bombarded by H atoms during deposition most of the diamond surface is H-terminated and is thus unreactive to incoming hydrocarbon radicals. This high fractional termination of surface sites is necessary to prevent surface reconstruction, graphitization and reactive etching back into the gas phase under the prevailing process conditions.

The present study is one part of a program aimed at providing more direct and quantitative measures of the both production and loss processes of H atoms and CH₃ radicals in a typical HF-CVD reactor. Both transient species are detected, in situ, and with sub millimeter spatial resolution, by 2 + 1 resonance enhanced multiphoton ionization (REMPI) spectroscopy using laser wavelengths ~243.1 [4] and ~333 nm [5–7], respectively. Here we concentrate on spatially resolved measurements of H atom and CH₃ radical relative number densities in the vicinity of the HF, as a function of process gas hydrocarbon (CH_4 and C_2H_2), process gas pressure and mixing ratio, and filament temperature. The results, which we compare with other spatially resolved studies of the gas phase chemistry prevail-

ing in such reactors [8–14], and with complementary HF-CVD modelling studies [15,16], serve to highlight the very different production routes for H atoms and CH_3 radicals in such a reactor, and help clarify some of the remaining uncertainties in our understanding of CH_3 radical production when using C_2H_2 as a process gas.

2. Experimental

The apparatus and procedures have been described previously [4] and are just summarized here. The CVD chamber comprises an evacuable six-way cross (base pressure $\sim 10^{-2}$ Torr). Two side arms are equipped with quartz windows to allow entry and exit of the probe laser beam. A third window, in the same horizontal plane, provides an observation port through which the HF may be viewed with a two colour optical pyrometer (Land Infrared). The HF (250 μm diameter Ta wire, seven turns, ~ 3 mm coil diameter) and, when appropriate, a substrate heater plate are both mounted on a cradle suspended beneath a linear transfer mechanism attached to the top flange, which is also equipped with the necessary electrical feed-throughs. The substrate heater plate was not present for any of the measurements reported herein. Attached to the mechanism is a pair of digital callipers, which permit positioning of the cradle with sub-millimetre precision. This allows the entire reactor assembly to be translated vertically by ≤ 25 mm relative to the fixed laser focus and REMPI probe, thereby enabling spatially resolved profiling of the chosen species. The cradle can also be rotated through any angle to allow measurements to be carried out along, or perpendicular to, the filament axis. Power is supplied to the HF (one terminal of which is grounded) via the feed-throughs, from a DC power supply (Isotech IP1810H) generally operated in constant current mode. The reagent gases, CH_4 (or C_2H_2) and H_2, are metered using separate mass flow controllers (Tylan), pre-mixed in a manifold and then enter the reactor through a port located above the cradle assembly; typical flow rates and operating pressures are 100 sccm (total) and 20 Torr, respectively.

H atoms are detected by $2 + 1$ REMPI on the $2s \leftarrow 1s$ transition using 243.1 nm radiation generated by a Nd-YAG pumped dye laser (Quanta-Ray DCR-2A plus PDL-3) operating at 10 Hz, using the dye coumarin 480 and subsequent frequency doubling (in BBO) with a home built 'autotracker'. The same laser, now operated with a DCM/LDS698 dye mixture and KDP crystal was used to generate wavelengths ~ 333 nm necessary for $2 + 1$ REMPI detection of CH_3 radicals via the origin band of the $3p_z;^2A_2'' \leftarrow \tilde{X}^2A_2''$ two photon transition [5–7]. In both cases the UV light is separated from the dye fundamental using a Pellin–Broca prism, attenuated to energies <100 μJ pulse^{-1} for H atom detection (<1 mJ pulse^{-1} for CH_3 radical detection) and focused into the centre of the reactor using a 20 cm f.l. quartz lens. A fraction of the UV light exiting the reactor is

diverted into a cuvette containing dilute Rhodamine 6G solution using a quartz beamsplitter, and the resulting fluorescence monitored by a photodiode for power-normalization purposes. Frequency calibration of the CH_3 REMPI spectra was achieved by recording, simultaneously, transitions of atomic neon excited in an optogalvanic lamp (using the fundamental dye laser output), while the frequency dispersion of the H atom excitation spectra was determined by directing part of the fundamental dye laser beam through an etalon and recording interference fringes (with a separation of 1.250(4) cm^{-1} in the visible). Positive ions formed in the probe volume are collected on a 750 μm diameter Pt wire probe maintained at -48.5 V, the end of which is positioned ~ 1.5 mm from the laser focus. The transient REMPI current signal and that from the photodiode monitoring UV power are passed to a digital oscilloscope (LeCroy 9361) and hence, via a GPIB interface, to a PC for storage and subsequent analysis. A second photodiode is used to monitor the etalon transmission in the visible; its output is fed via a linear gate (SRS 250) to the PC.

3. Results and discussion

Fig. 1a,b show representative H atom $2s \leftarrow 1s$ two photon transition lineshapes recorded in 20 Torr of pure H_2 with the laser focus at $d = 0.5$ and 10 mm from the bottom of the hot coiled Ta filament held at $T_{fil} = 2375$ K. The smooth curve through each data set is a least squares fit to a Gaussian function. The line broadening is dominated by Doppler broadening; after deconvoluting the laser bandwidth (0.07 cm^{-1} FWHM in the UV), the resulting FWHM values ($\Delta \nu_D$) provide a measure of the translational temperature of the gas in the locality of the laser focus via the relationship

$$\Delta \nu_D = \frac{\nu_0}{c} \sqrt{\frac{8kT \ln 2}{M}} \tag{1}$$

where ν_0 is the line centre transition frequency, c the speed of light and M the mass in kg [4]. Given that both lineshapes were recorded at the same incident laser pulse energy, their respective areas provide measures of the relative H atom number densities in the focal volume. Fig. 1d shows a representative $2 + 1$ REMPI spectrum of the $CH_3(3p_z;^2A_2'' \leftarrow \tilde{X}^2A_2'')$ transition obtained using a 1% CH_4 in H_2 gas mixture at a distance $d = 4$ mm from the hot filament maintained at 2475 K. The strong feature at an excitation wavelength ~ 333 nm is dominated by the Q branch of the origin band transition, while the weaker feature at higher wavenumber is attributable to the 2_1^1 hot band of this same electronic transition [5]. The smooth curve above the former feature (Fig. 1c) is a simulation of the origin band contour. This employs the appropriate zero and second rank tensor components to describe the two photon transition amplitude (with relative weightings 1:2.5), spectroscopic constants $\nu_0 = 59955$ cm^{-1}, $B' = 9.51$ cm^{-1} and $C' = 4.62$ cm^{-1} for the excited ($3p_z;^2A_2''$) electronic state, [7] (the quartic
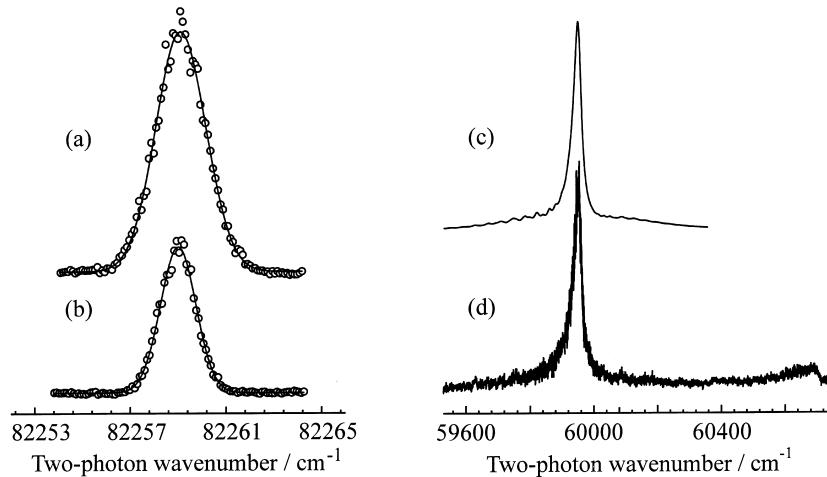
Fig. 1. Representative Doppler lineshapes of the H atom 2s ← 1s two photon transition recorded in 20 Torr of pure H_2 with the laser focus at (a) $d = 0.5$ and (b) $d = 10$ mm from the bottom of the hot coiled Ta filament held at $T_{fil} = 2375$ K. The solid curve in each case is a least squares fit to a Gaussian function, the FWHMs of which (after deconvolution of the laser linewidth) yield a measure of the local temperature ~1750 and ~840 K, respectively), while the areas under such lineshapes provide a measure of the relative H atom number density.

distortion constants were all set to the corresponding ground state values), literature values for the ground ($\tilde{X}^2A_2''$) state spectroscopic constants [17], an excited state predissociation that scales with the N' and K' rotational quantum numbers as parameterized by Heinze et al., [7] a predissociation broadened linewidth of $\Delta\nu = 12$ cm^{-1} for transitions involving the rotationless $N' = K' = 0$ level, and a rotational temperature of 1150 K. Full details of these band contour simulations will be presented in a future publication.

Given experimental data such as these we are in a position to map out spatially resolved temperature, and H atom and CH_3 radical number density, profiles within the hot filament reactor, as a function of process conditions. Fig. 2a illustrates the way in which the H atom number density at $d = 1$ mm, at a constant 100 sccm flow rate of pure H_2, varies as a function of H_2 pressure, $p(H_2)$, in the range 5–

55 Torr. The observed invariance to $p(H_2)$ implies an H atom formation process that is zero-order with respect to H_2 number density. Such has been rationalized by assuming that the dominant H atom formation mechanism involves dissociative adsorption of H_2 on the surface of the hot filament. Fig. 2b shows a plot of CH_3 REMPI signal, measured at $d = 4$ mm, plotted as a function of the percentage of CH_4 in a CH_4/H_2 gas mix. CH_4 addition leads to filament carburization and a concomitant increase in filament resistance. To maintain a constant T_{fil} (as measured by the optical pyrometer) it was thus necessary to reduce progressively the power supplied to the filament as the hydrocarbon content was increased. The important feature to note from this plot is that, in accord with several previous measurements, [11,18,19] and in contrast to the H atom data shown in Fig. 2a, the measured signal (and thus CH_3 relative number
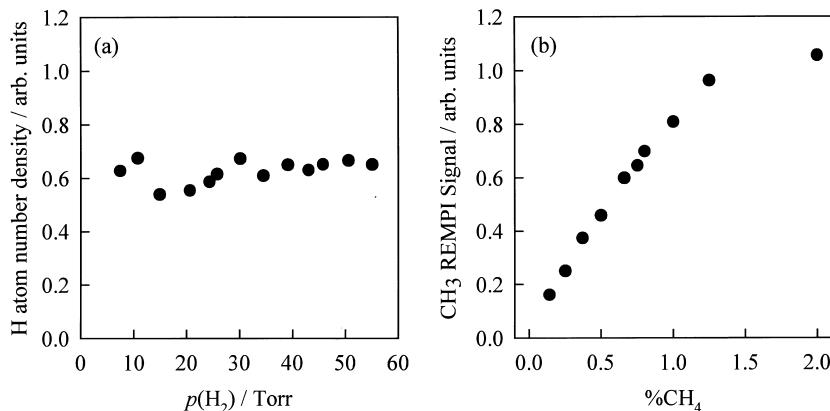
Fig. 2. (a) H atom relative number densities measured at $d = 1$ mm, at a constant 100 sccm flow rate of pure H_2 and with $T_{fil} = 2375$ K, plotted as a function of H_2 pressure, $p(H_2)$; (b) 2 + 1 REMPI signal measured at the peak of the $CH_3(3p_z; {}^2A_2'' \leftarrow \tilde{X}^2A_2'')$ origin band contour, at $d = 4$ mm, using a constant 100 sccm flow rate of H_2 at 20 Torr pressure, together with various percentages of added CH_4.
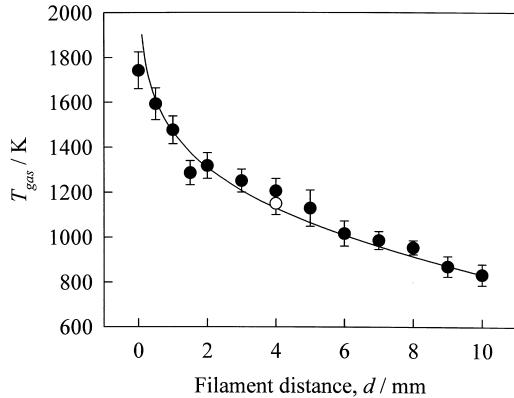
Fig. 3. Local gas temperatures in 20 Torr of pure H_2 with $T_{fil} = 2360$ K, as deduced from analysis of the H atom $2s \leftarrow 1s$ two photon Doppler lineshapes ($\bullet$), plotted as a function of d. The open circle shows the rotational temperature deduced by simulating the contour of the measured $2 + 1$ REMPI spectrum of the CH_3 origin band at $d = 4$ mm (Fig. 1c,d), while the smooth curve is a fit to the data using Eq. (2).

density) increases with increasing CH_4, at least up to 2% CH_4 content. Similar trends in CH_3 relative number density were observed when using C_2H_2/H_2 process gas mixtures.

Spatially resolved measurements of species number densities requires knowledge of the local gas temperature. As Fig. 1 showed, the H atom Doppler profiles are sensitive to the local gas temperature. So, too, is the detailed form of the rotational contour of the CH_3 origin band (Fig. 1c,d). Fig. 3 illustrates the good agreement between the d dependence of the H atom translational temperature deduced from Doppler lineshape analysis (filled circles) [4] and the CH_3 rotational temperature determined at $d = 4$ mm from band contour analysis (Fig. 1d; shown by the open circle). The solid line through the data points in this figure is obtained using Eq. (2), which derives from 2D diffusive calculations [15] involving solution of the conservation equations for mass, momentum, energy and species concentration, and the assumption that conduction is the dominant heat transport mechanism

$$T_d = T_{d=0}\{1 - [1 - (T_L/T_{d=0})^2]\ln(d/R_f)\ln(L/R_f)\}^{0.5} \quad (2)$$

where $T_{d=0}$ and T_L are the gas temperature very close to the filament and at a distance L from the filament, respectively, and R_f is the filament radius (125 μm).

The remainder of this article is concerned with CH_3 relative number density measurements as a function of, e.g. position (d) or filament temperature (T_{fil}). Fig. 4 demonstrates that both the H atom number density and the measured CH_3 REMPI signal, measured at $d = 4$ and 2 mm, respectively, rise rapidly with increasing T_{fil}. A van't Hoff plot of the former data is linear, with a gradient that implies a dissociation enthalpy $\Delta H_{diss} \sim 228$ kJ mol^{-1}, in close accord with the value for the gas phase reaction

$$H_2 \rightleftharpoons 2H \quad (3)$$

in the corresponding temperature range [4]. This, the finding

that the H atom number density is greatest at $d = 0$, [4,11,12,20] and the observed insensitivity of the H atom number density to $p(H_2)$, all serve to indicate that the key role of the filament surface is to provide an efficient means whereby H_2 molecules can attain T_{fil} and hence establish an extent of dissociation appropriate to that temperature.

The measured CH_3 REMPI signal rises less steeply with increasing T_{fil}. However, two correction factors must be applied in any such situation where the gas temperature is a variable in order to convert a REMPI signal measured at just one wavelength within the CH_3 ($3p_z$; $^2A_2'' \leftarrow \tilde{X}^2A_2''$) origin band into a relative number density of CH_3 radicals. The first recognizes that the origin band contour is itself a temperature dependent function [7], and that measurements made at any one REMPI probe laser wavelength will thus sample a temperature dependent fraction of the total REMPI signal. This temperature dependent sampling efficiency can be accommodated by calculating the CH_3 ($3p_z$; $^2A_2'' \leftarrow \tilde{X}^2A_2''$) origin band rotational contour for a range of temperatures in the range $600 < T_{gas} < 1700$ K and then determining the relative fraction that falls within the bandwidth of the REMPI probe laser centred at 59 950 cm^{-1} and assumed Gaussian. In practice, the dominant Q branch shows little degradation, and the correction factor, f_C, by which the measured REMPI signals must be divided in order to account for the temperature dependence of the band contour (which we scale so that $f_C = 1$ at $d = 4$ mm and $T_{gas} = 1150$ K), only decreases from 1.08 to 0.90 over the temperature range 600–1700 K (see Fig. 5).

The second, more substantial, correction recognizes the temperature dependence of the vibrational partition function. The CH_3 radical has two singly degenerate fundamental modes of vibrational (the symmetric stretch vibration $\nu_1 = 3004.4$ cm^{-1} and the out-of-plane bend, $\nu_2 = 606.5$ cm^{-1} in the ground electronic state) and two doubly degenerate modes, the asymmetric stretch $\nu_3 = 3160.8$ cm^{-1} and the in-plane bend $\nu_4 \sim 1400$ cm^{-1} [21]. The relative populations of these vibrational states, and thus the fraction of the
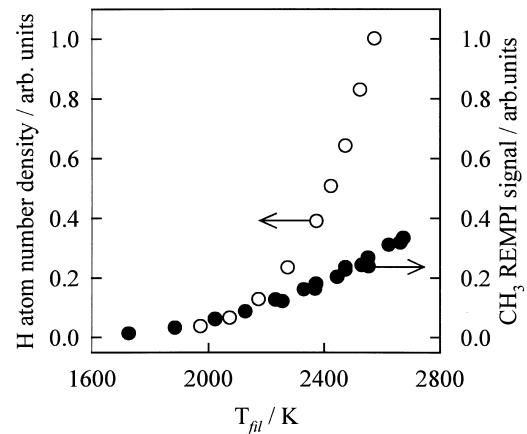
Fig. 4. H atom relative number densities ($\bigcirc$) and CH_3 REMPI signal intensities ($\bullet$) measured at, respectively, $d = 4$ and 2 mm, and 20 Torr pressure, plotted as a function of T_{fil}.
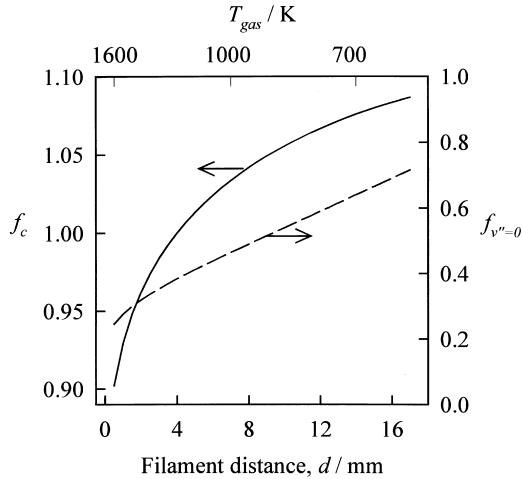
Fig. 5. Plots illustrating the T_{gas} dependence of the relative sampling efficiency, f_C, for CH_3 radicals by REMPI at a two photon energy of 59950 cm^{-1} (left hand scale), and the fraction of the total CH_3 radical population in the zero-point vibrational level, $f_{v''=0}$ (right hand scale).

total CH_3 radical population that is in the ground vibrational level, $f_{v''=0}$, will depend on T_{gas}. Fig. 5 also illustrates the temperature dependence of $f_{v''=0}$, calculated assuming (i) local thermodynamic equilibrium amongst the various degrees of freedom and (ii) that the six normal modes of vibration may all be approximated as harmonic oscillators. Clearly, $f_{v''=0}$ declines by more than a factor of two over the range $600 < T_{gas} < 1700$ K. The measured CH_3 REMPI signals will only provide a reliable measure of the total CH_3 relative number density if population in all of the populated vibrational states is sampled with equal efficiency. In the case of the $CH_3(3p_z;\ ^2A_2'' \leftarrow \tilde{X}^2A_2'')$ transition this is obviously not so, since the frequency of the out-of-plane bending vibration ν_2 – which, by virtue of its low frequency, participates in most of the thermally populated levels with $\nu'' > 0$ – increases dramatically upon electronic excitation (from 606.5 cm^{-1} to $\sim$1334 cm^{-1} [5]). This, together with

the Franck–Condon requirement that $\Delta \nu_2 =$ even, ensures that all of the more significant hot band transitions in the $2 + 1$ REMPI spectrum of CH_3 will be blue shifted with respect to the origin band [5]. Thus, the measured CH_3 REMPI signals (which we now consider to provide a measure of the $\nu'' = 0$ population only) must be scaled to reflect the trend in $f_{v''=0}$ (T) shown in Fig. 5 in order to obtain total CH_3 relative number densities.

Fig. 6 shows the radial dependence of the measured CH_3 REMPI signals obtained using gas mixtures comprising of (a) 1% CH_4 in H_2 and (b) 0.5% C_2H_2 in H_2, both at total pressures of 20 Torr, a gas flow rate of 100 sccm and $T_{fil} = 2475$ K, together with our best estimates of the d dependence of the total CH_3 number density after inclusion of the temperature dependent corrections for f_C and $f_{v''=0}$ described above. Both of the measured CH_3 radial distribution functions (i.e. before correction) match well with that reported by Kruger, Zare and coworkers, [13,14] who used cavity ring down spectroscopy (CRDS) to monitor the CH_3 column density (via the 3s; $\tilde{B}^2A_1' \leftarrow \tilde{X}^2A_2''$ origin band at 213.9 nm) in a hot filament activated CH_4/H_2 gas mixture. The observation, that the CH_3 signal maximizes at $d > 0$, i.e. away from the filament, is in marked contrast to the measured H atom number density [4,11,12,20]. Nonetheless, the qualitative form of the radial profile of the CH_3 signal is readily explicable [16] once it is recognized that the CH_3 number density is largely determined by the gas phase equilibrium

$$H + CH_4 \rightleftharpoons CH_3 + H_2 \qquad (4)$$

and that, although the H atom number density decreases monotonically with increasing d, the total gas number density (and thus the CH_4 number density) increases with d due to the inverse dependence between number density and T_{gas} (at constant pressure). The present data suggests that the apparently excellent agreement between the CRDS data [13,14] and theory [16] may be somewhat fortuitous, however. The CRDS measurements return column densities, along which there is inevitably a marked
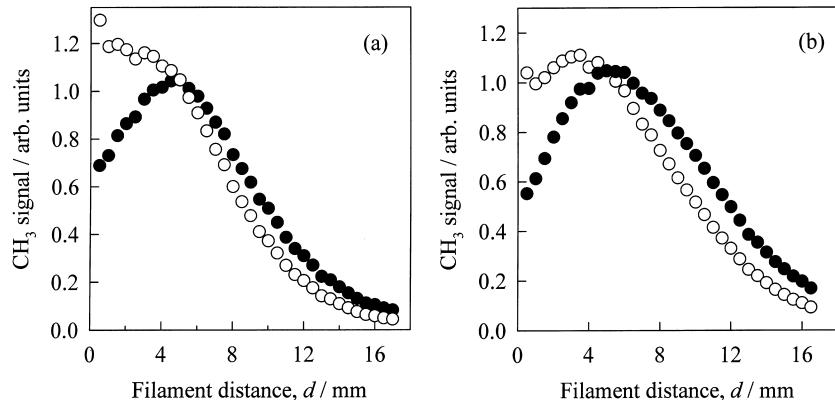
Fig. 6. CH_3 REMPI signals (●) measured as a function of d using (a) 1% CH_4 in H_2 and (b) 0.5% C_2H_2 in H_2 gas mixtures, 20 Torr pressure, 100 sccm gas flow rate and $T_{fil} = 2475$ K. The open symbols (○) show the d dependence of the total CH_3 relative number density obtained by scaling the measured REMPI signals applying the temperature dependent sensitivity factors f_C and $f_{v''=0}$.

temperature variation. Just as in the present study, the absorbances measured by CRDS will necessarily be sensitive to any temperature dependence in f_C and $f_{\nu''=0}$ (the monitoring wavelength was chosen because of the reported temperature invariance of the CH_3 absorption cross-section of 213.9 nm [22]). Absorption measurements at this wavelength are also prone to contamination by overlapping contributions from hot bands of C_2H_2, [10] which arises whenever CH_4/H_2 gas mixtures are used for diamond CVD. Both the total C_2H_2 number density and the fraction of the population contributing to long wavelength hot band absorption will depend on T_{gas}, and thus vary along the column length.

Despite these differences in detail, one major finding of the present REMPI study, the previous CRDS studies [13,14] and the related reactor modelling studies [16] remains unchallenged: CH_3 radicals arising in a hot filament activated CH_4/H_2 gas mixture arise primarily via the gas phase equilibrium (Eq. (4)) [3]. The current understanding regarding CH_3 radical formation when using hot filament activated C_2H_2/H_2 gas mixtures is much less clear cut. Numerous studies have demonstrated that CVD diamond may be grown, with comparable quality and efficiency, using either CH_4 or C_2H_2 as the carbon precursor. A variety of in situ studies have demonstrated C_2H_2 conversion into CH_4, that the C_2H_2/CH_4 mixing ratio at typical process temperatures is essentially independent of the hydrocarbon feedstock gas used, [9,23–26] and the presence of CH_3 radicals [10]. These latter workers [10] discussed possible gas phase and surface catalyzed routes for converting C_2H_2 to CH_3 but were unable to distinguish which, if either, was the dominant contributor to the measured CH_3 concentrations. Zumbach et al. [26] compared measured $C_2H_2/C_2H_4/C_2H_6$ concentration ratios in a hot filament activated C_2H_2/H_2 gas mixture with the output of model calculations which included only gas phase chemistry. These simulations suggested no conversion from C_2H_2 to any other hydrocarbon, in marked contradiction to the experimental observation; it was therefore concluded, [26] almost by default, that C–C bond breaking must involve adsorption, hydrogenation and subsequent desorption on hot surfaces within the reactor. Goodwin and Butler, [3] having reviewed the available thermodynamic and kinetic data pertaining to the various C_2H_x hydrocarbon species, ultimately reach a similar conclusion that heterogeneous conversion on the reactor walls (or even on the growing diamond surface) is the most likely route for C–C bond breaking.

The present data suggests that such conclusions need some further review. The present experiments involved no hot diamond substrate, and the reactor walls are both remote and cold. The measured CH_3 number density variations with hydrocarbon/H_2 mixing ratio, with T_{fil} and as a function of radial distance from the filament, d, show little sensitivity to whether the carbon is initially introduced as CH_4 or C_2H_2. All are most readily accommodated in terms of gas phase chemistry, involving H atoms and the hydrocarbon precursor. Clearly, the endoergicity of the forward reaction

$$H + C_2H \rightleftharpoons C_2H + H_2 \tag{5}$$

mitigates against this simple H atom abstraction process being an important step in the route to C–C bond fission, but Toyoda et al. [10] have argued that a sequence of H and H_2 addition steps along the lines of

$$C_2H_2 + H + M \rightleftharpoons C_2H_3 + M \tag{6a}$$

$$C_2H_4 + H + M \rightleftharpoons C_2H_5 + M; \qquad \text{etc.} \tag{6b}$$

($*C_2H_4 + H$; $CH_3 + CH_2$; etc) could provide a purely gas phase route to C–C bond cleavage. We note that, simply on probability grounds, the third body M will most likely be H_2, which is the reactant needed to drive the reaction through to the exothermic products (Eq. (6b)). Current and future REMPI studies in our group will investigate further aspects of the gas phase chemistry (e.g. the way the CH_3 number density arising in both CH_4/H_2 and C_2H_2/H_2 gas mixtures varies with H_2 partial pressure), and gas-surface chemistry, most notably the way in which both H atom and CH_3 radical number densities near a diamond surface vary as a function of that surface temperature.

4. Conclusions

2 + 1 REMPI spectroscopy has enabled spatially resolved in situ measurements of H atom and CH_3 radical relative number densities and the local gas temperature in a hot filament reactor used for diamond chemical vapour deposition (CVD). H atom number densities are observed to maximize at the hot filament surface, to be independent of the H_2 pressure in the range 5–55 Torr, and to drop monotonically with increasing radial distance from the filament, d. By way of contrast, the CH_3 radical number density arising both in dilute CH_4/H_2 and C_2H_2/H_2 gas mixtures is found to increase with the hydrocarbon input gas pressure and filament temperature, but to be rather constant for $d < 4$ mm and to decline thereafter. These direct measurements serve to reinforce the view that H atom production during diamond CVD in a hot filament reactor arises as a result of dissociative adsorption on the hot filament surface, whereas CH_3 radical formation in the case of CH_4/H_2 process gas mixtures is dominated by gas phase reactions. The CH_3 number density profiles we observe when using CH_4 and C_2H_2 are strikingly similar. This suggests that CH_3 radicals formed in activated C_2H_2/H_2 gas mixtures also arise as a result of homogeneous gas phase chemistry, in contradiction of the current consensus which invokes surface catalyzed hydrogenation to enable the necessary C–C bond fission step.

References

[1] J.E. Field (Ed.), The Properties of Natural and Synthetic Diamond, Academic Press, London, 1992, p. 710.

[2] B. Dischler, C. Wild (Eds.), Low-Pressure Synthetic Diamond, Springer-Verlag, Berlin, 1998, p. 384.

[3] D.G. Goodwin, J.E. Butler, in: M.A. Prelas, O. Popovici, L.K. Bigelow (Eds.), Handbook of Industrial Diamonds and Diamond Films, Marcel Dekker, New York, 1998, pp. 527–580.

[4] S.A. Redman, C. Chung, K.N. Rosser, M.N.R. Ashfold, Phys. Chem. Chem. Phys. 1 (1999) 1415.

[5] J.W. Hudgens, T.G. DiGuiseppe, M.C. Lin, J. Chem. Phys. 79 (1983) 571.

[6] R. Ogorzalek Loo, H.-P. Haerri, G.E. Hall, P.L. Houston, J. Chem. Phys. 90 (1989) 4222.

[7] J. Heinze, N. Heberle, K. Kohse-Höinghaus, Chem. Phys. Lett. 223 (1994) 305.

[8] F.G. Celii, J.E. Butler, J. Appl. Phys. 71 (1992) 2877.

[9] E.J. Corat, D.G. Goodwin, J. Appl. Phys. 74 (1993) 2021.

[10] H. Toyoda, M.A. Childs, K.L. Menningen, L.W. Anderson, J.E. Lawler, J. Appl. Phys. 75 (1994) 3142.

[11] M.A. Childs, K.L. Menningen, L.W. Anderson, J.E. Lawler, J. Chem. Phys. 104 (1996) 9111.

[12] L.L. Connell, J.W. Fleming, H.-N. Chu, D.J. Vesteck Jr., E. Jensen, J.E. Butler, J. Appl. Phys. 78 (1995) 3622.

[13] P. Zalicki, Y. Ma, R.N. Zare, E.H. Wahl, T.G. Owano, C.H. Kruger, Appl. Phys. Lett. 67 (1995) 144.

[14] E.H. Wahl, T.G. Owano, C.H. Kruger, P. Zalicki, Y. Ma, R.N. Zare, Diam. Rel. Mater. 5 (1996) 373.

[15] Y.A. Mankelevich, A.T. Rakhimov, N.V. Suetin, Diam. Rel. Mater. 5 (1996) 888.

[16] Y.A. Mankelevich, N.V. Suetin, A.T. Rakhimov, Diam. Rel. Mater. 7 (1998) 1133.

[17] C. Yamada, E. Hirota, K. Kawaguchi, J. Chem. Phys. 75 (1981) 5256.

[18] W.L. Hsu, Appl. Phys. Lett. 59 (1991) 1427.

[19] M.A. Childs, K.L. Menningen, P. Chevako, N.W. Spellmeyer, L.W. Anderson, J.E. Lawler, Phys. Lett. A 171 (1992) 87.

[20] U. Meier, K. Kohse-Höinghaus, L. Schafer, C.-P. Klages, Appl. Optics 29 (1990) 4993.

[21] M.E. Jacox, J. Phys. Chem. Ref. Data 27 (1998) 115, and references therein.

[22] S.M. Hwang, M.J. Rabinowitz, W.C. Gardiner Jr., Chem. Phys. Lett. 205 (1993) 157.

[23] C.H. Wu, M.A. Tanor, T.J. Potter, E.W. Kaiser, J. Appl. Phys. 68 (1990) 4825.

[24] M.C. McMaster, W.L. Hsu, M.E. Coltrin, D.S. Dandy, J. Appl. Phys. 76 (1994) 7567.

[25] C.A. Rego, R.S. Tsang, P.W. May, M.N.R. Ashfold, K.N. Rosser, J. Appl. Phys. 79 (1996) 7264.

[26] V. Zumbach, J. Schafer, J. Tobai, et al., J. Chem. Phys. 107 (1997) 5918.